RESEARCH ARTICLE

National Science Review
7: 64–72, 2020
doi: 10.1093/nsr/nwz070
Advance access publication 11 June 2019

MATERIALS SCIENCE

Scalable fabrication of printed Zn//MnO_2 planar micro-batteries with high volumetric energy density and exceptional safety

Xiao Wang[1,2], Shuanghao Zheng[1,2,3], Feng Zhou[1], Jieqiong Qin[1,2], Xiaoyu Shi[1,3,4], Sen Wang[1,2], Chenglin Sun[1], Xinhe Bao[1,3,4] and Zhong-Shuai Wu[1,*]

ABSTRACT

The rapid development of printed and microscale electronics imminently requires compatible micro-batteries (MBs) with high performance, applicable scalability, and exceptional safety, but faces great challenges from the ever-reported stacked geometry. Herein the first printed planar prototype of aqueous-based, high-safety Zn//MnO_2 MBs, with outstanding performance, aesthetic diversity, flexibility and modularization, is demonstrated, based on interdigital patterns of Zn ink as anode and MnO_2 ink as cathode, with high-conducting graphene ink as a metal-free current collector, fabricated by an industrially scalable screen-printing technique. The planar separator-free Zn//MnO_2 MBs, tested in neutral aqueous electrolyte, deliver a high volumetric capacity of 19.3 mAh/cm^3 (corresponding to 393 mAh/g) at 7.5 mA/cm^3, and notable volumetric energy density of 17.3 mWh/cm^3, outperforming lithium thin-film batteries ($\leq$10 mWh/cm^3). Furthermore, our Zn//MnO_2 MBs present long-term cyclability having a high capacity retention of 83.9% after 1300 cycles at 5 C, which is superior to stacked Zn//MnO_2 batteries previously reported. Also, Zn//MnO_2 planar MBs exhibit exceptional flexibility without observable capacity decay under serious deformation, and remarkably serial and parallel integration of constructing bipolar cells with high voltage and capacity output. Therefore, low-cost, environmentally benign Zn//MnO_2 MBs with in-plane geometry possess huge potential as high-energy, safe, scalable and flexible microscale power sources for direction integration with printed electronics.

Keywords: low cost, printed, planar, Zn//MnO_2 micro-batteries, metal-free current collectors

[1]Dalian National Laboratory for Clean Energy, Dalian Institute of Chemical Physics, Chinese Academy of Sciences, Dalian 116023, China; [2]University of Chinese Academy of Sciences, Beijing 100049, China; [3]State Key Laboratory of Catalysis, Dalian Institute of Chemical Physics, Chinese Academy of Sciences, Dalian 116023, China and [4]Department of Chemical Physics, University of Science and Technology of China, Hefei 230026, China

*__Corresponding author__. E-mail: wuzs@dicp.ac.cn

Received 15 April 2019; **Revised** 20 May 2019; **Accepted** 26 May 2019

INTRODUCTION

The emerging smart printed electronics with the integrated features of exceptional flexibility, thinness, light weight, and miniaturization have significantly inspired the relentless pursuit of low-cost, safe and environmentally benign printed microscale energy-storage devices with high performance [1–5]. Lithium thin-film micro-batteries (MBs) with energy density of 10 mWh/cm^3 are the most popular microscale power sources for various microsystems. However, most reported MBs are usually constructed in a non-planar stacked geometry, resulting in bulky volume, limited flexibility, and inconvenient serial and parallel connection via metal interconnects. Also, such MBs are generally fabricated by complicated manufacture processes, e.g. the photolithographic technique, and present unsatisfactory safety issues with flammable organic electrolytes. To overcome this, aqueous-based printed MBs with a separator-free planar geometry is acknowledged as a highly competitive class of microscale power sources due to the intrinsic non-flammability, high ionic conductivity of aqueous electrolytes [5,6], and great advances of planar device geometry with extremely short ion-diffusion pathways [7,8]. It is noteworthy that the printed planar MBs are highly favorable for direct integration of printed electronics on a single substrate, simultaneously combining the characteristics of outstanding flexibility, designable shapes, adjustable sizes, and space-saving connections.

So far, various printing techniques have been developed for fabricating traditional stacked batteries [9–12], such as lithium ion batteries by 3D printing [11], Zn–Ag batteries by inkjet printing [13], and Zn–air batteries by screen printing [14]. Also, great progress has been made with planar lithium thin-film MBs [15], lithium-ion MBs [16], Zn//Ag_2O [3], Zn//$LiMn_2O_4$ [17], Zn//$LiFePO_4$ [17], 3D MBs [18–20], and micro-supercapacitors [21–24] through the development of various microfabrication techniques, such as photolithography [25], electrodeposition [26], spraying [9,27], laser scribing [28], mask-assisted filtration [16], inkjet printing [10], roll-to-roll printing [29], and 3D printing [11,12]. In particular, screen printing can effectively control the precise pattern design with adjustable rheology of the inks, and is very promising for large-scale application [29]. Besides, screen printing is recognized as a cost-effective, easy-processing, and mass-production methodology for the fast construction of MBs, having precise control over the performance, flexibility, and integration with printed microelectronics. To address the cost effectiveness and safety issues, aqueous rechargeable Zn//MnO_2 batteries, characterized by high abundance, low cost, non-toxicity and safety of both Zn and MnO_2, as well as high output voltage of 0.9–1.8 V in aqueous electrolyte and high capacity of 820 mAh/g [30–32], are rising as one of the most compelling candidates [33–36]. Nevertheless, low-cost and scalable fabrication of aqueous-based Zn//MnO_2 planar MBs with multiple innovative form factors of high performance, flexibility, and integration still remains challenging.

Herein we report a cost-effective and industrially applicable screen-printing strategy for fast and scalable production of rechargeable Zn//MnO_2 planar MBs, featuring high performance, superior flexibility, scalable applicability, and high safety. The Zn//MnO_2 planar MBs, free of separators, were manufactured by directly printing the zinc ink as the anode (thickness of 6.4 μm) and γ-MnO_2 ink as the cathode (thickness of 9.8 μm), high-quality graphene ink as metal-free current collectors, working in environmentally benign neutral aqueous electrolytes of 2 M $ZnSO_4$ and 0.5 M $MnSO_4$. Benefiting from the suitable rheological properties of the inks and high electrical conductivity of microelectrodes (463 S/m for zinc anode, and 339 S/m for MnO_2 cathode), the as-fabricated Zn//MnO_2 MBs showed outstanding volumetric capacity of 19.3 mAh/cm^3 at 7.5 mA/cm^3 (393 mAh/g at 154 mA/g), high energy density of 17.4 mWh/cm^3, long-term cycling stability (~83.9% after 1300 times at 5 C), designable shape, extraordinary flexibility, outstanding serial and parallel modularization for boosting the capacity and voltage output. Therefore, taking such impressive performance into account, our Zn//MnO_2 MBs fabricated with screen-printing technology could potentially meet the stringent requirements of high performance, environmental friendliness, low cost, easy scalability, and high safety for printed electronics [37].

RESULTS AND DISCUSSION

The screen-printing fabrication of the interdigital Zn//MnO_2 planar MBs is schematically illustrated in Fig. 1a–h. Firstly, highly stable and conductive graphene ink with appropriate rheological properties was printed on the substrates, e.g. flexible polyethylene terephthalate (PET), cloth, A4 paper, and even rigid glass (Fig. 1i–k), through a screen-printed process to form the interdigital planar patterns as metal-free current collectors, with a typical thickness of 1.4 μm, and exceptional electrical conductivity of 2.3 × 10^4 S/m (Fig. S1a, Supporting Information). Secondly, the anodic four fingers of asymmetric interdigital microelectrodes were deposited by extruding Zn-based ink (33.3 wt% Zn microparticles) (Fig. 2a, Figs S2a and S3a, b, Supporting Information) through the screen on one side of the four graphene current collectors. Thirdly, the cathodic four fingers were manufactured by screen-printing γ-MnO_2-based ink (18.8 wt% MnO_2 nanoparticles) (Fig. 2b, Figs S2b, S3c, d, and S4, Supporting Information) on the other side of the four graphene-based current collectors. Notably, all inks possessed typical thixotropic behavior, showing a decreasing viscosity with increasing shear rate, staying below 1 Pa·s from 10 to 8000 s^{-1} (Fig. S5a–c, Supporting Information), which is highly important for precisely patterning microelectrodes [37,38]. The screen-printed Zn-based anode and MnO_2-based cathode (SEM, Fig. S6, Supporting Information), with a typical thickness of 6.4 and 9.8 μm (Fig. 2c–f), exhibited high electrical conductivity of ~320 and ~450 S/m (Fig. S1b–c, Supporting Information), respectively. It is noted that the as-fabricated Zn//MnO_2 planar MBs, free of both the separator and metal current collectors, exhibited extremely short ion-diffusion distances [39–42], and robust flexibility without film fracture and delamination from the substrate under various bending states (Fig. 2g–m) [8]. Furthermore, our screen-printing technique is highly simple, effective and scalable for low-cost production of flexible and seamlessly integrated Zn//MnO_2 MBs with designable shapes and complex planar geometries, such as individual (Fig. 2g, j) and multiple parallel interdigital MBs via connection in series and in parallel (Fig. 2i, k), our institute logo MBs (Fig. 2h),

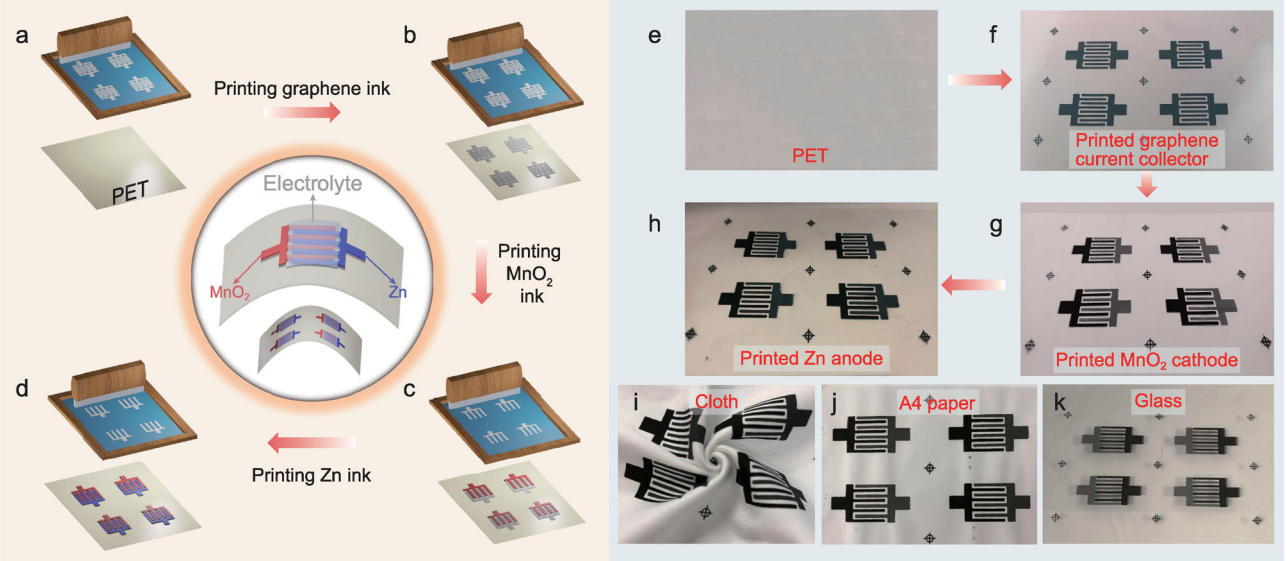

Figure 1. Fabrication of printed Zn//MnO_2 planar MBs. (a–d) Schematic of screen-printing fabrication of printed Zn//MnO_2 MBs: (a) the blank PET substrate, (b) the printed graphene current collectors, (c) the printed MnO_2 cathode and (d) the printed Zn anode. (e–h) Optical photographs showing the stepwise printing fabrication of Zn//MnO_2 MBs: (e) the blank PET substrate, (f) the graphene current collectors, (g) the printed MnO_2 cathode and (h) the printed Zn anode on interdigital graphene fingers. (i–k) Zn//MnO_2 MBs printed onto different substrates, including (i) cloth, (j) A4 paper, and (k) glass.

tandem concentric circular (Fig. 2l) and linear MBs (Fig. 2m) not requiring conventional metal-based interconnectors. Finally, after adding the aqueous electrolyte (2 M $ZnSO_4$ and 0.5 M $MnSO_4$) onto the projected area of microelectrodes and packaging, aqueous-based Zn//MnO_2 planar MBs were obtained.

To demonstrate the outstanding electrochemical performance, we first measured galvanostatic charge and discharge (GCD) profiles of printed Zn//MnO_2 MBs at different current densities of 0.5 to 5 C (1 C = 308 mA/g, or 15 mA/cm^3) between 0.9 and 1.8 V, using a neutral aqueous electrolyte containing 2 M $ZnSO_4$ and 0.5 M $MnSO_4$. It is pointed out that the presence of $MnSO_4$ can significantly prevent the dissolution of MnO_2 and improve the cyclability of Zn//MnO_2 MBs [42]. As expected, the addition of 0.5 M $MnSO_4$ into electrolyte indeed results in an impressively enhanced performance of Zn//MnO_2 MBs (Fig. S7a, b, Supporting Information) [42]. Apparently, our Zn//MnO_2 MBs displayed a similar discharge voltage plateau at ~1.3 V observed at different current densities (Fig. 3a), originating from the intercalation mechanism in Zn//MnO_2 MBs. Specifically, the insertion and extraction processes of both H^+ and Zn^{2+} in the cathode are formulated as follows [43]:

$$\text{Cathode: } MnO_2 + H^+ + e^- \leftrightarrow MnOOH$$

$$Zn^{2+} + 2MnO_2 + 2e^- \leftrightarrow ZnMn_2O_4$$

$$\text{Anode: } Zn \leftrightarrow Zn^{2+} + 2e^-$$

Regardless of the increased rates, it was observed that the polarization did not virtually increase at high discharge rates. Importantly, our MBs presented exceptionally high capacity at the different rates. It was revealed that the discharge capacity varies from 18.4 (5th cycle), 14.2 (15th cycle), 9.8 (25th cycle) to 7.7 (35th cycle) mAh/cm^3 with increasing rates from 0.5, 1, 3 to 5 C, respectively (Fig. 3b). Notably, the capacity thus readily returned to 9.6 (45th cycle), 13.6 (55th cycle) and 19.3 (65th cycle) mAh/cm^3 when the rates go back to 3, 1, and 0.5 C, respectively (Fig. 3b).

The long-term cycling stability of Zn//MnO_2 MBs is one of the most important performance metrics for actual applications. Through the elaborate screening of cathodic MnO_2 and anodic zinc powder, selection of aqueous electrolytes ($ZnSO_4 + MnSO_4$), processing of highly stable and conducting inks, and usage of metal-free graphene current collectors, together with advanced planar geometry with a shorter ion-diffusion pathway and free of separator, and a sophisticated screen-printing technique, synergistically working together, the resulting Zn//MnO_2 MBs showed remarkably satisfactory cycling performance (Fig. 3c, d, g). It is disclosed that the Zn//MnO_2 planar MBs displayed an impressive capacity of 15 mAh/cm^3 over 100 cycles at a low current density of 1 C. In sharp contrast, the stacked Zn//MnO_2 MBs based on sandwich-like Zn foil and MnO_2 electrode with a thickness of ~200 μm, prepared by conventional blade coating (MnO_2: acetylene black: polyvinylidene fluoride

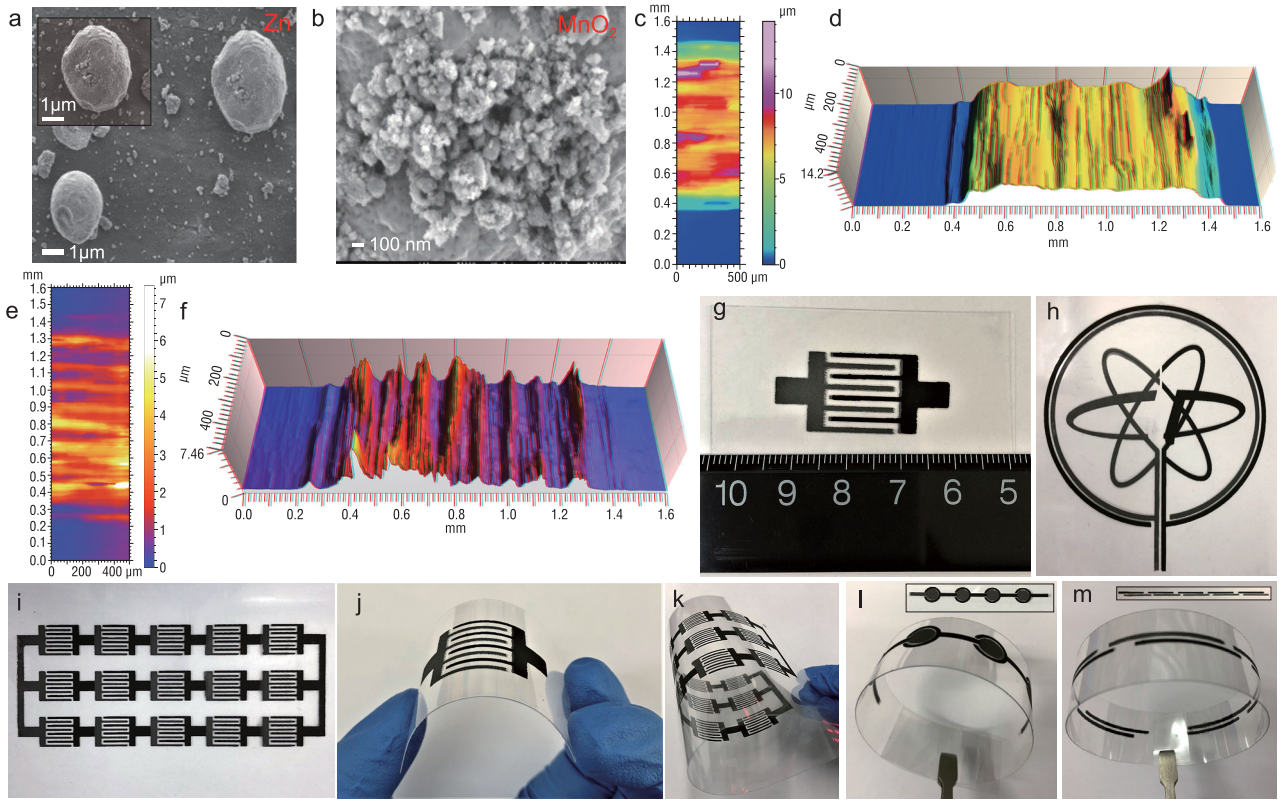

Figure 2. Characterization and shape diversity of printed Zn//MnO_2 planar MBs: SEM images of (a) Zn anode and (b) MnO_2 cathode; (c) 2D pseudo-color view and (d) 3D view of MnO_2 microelectrode finger on PET substrate, showing the microelectrode thickness of ~9.8 μm; (e) 2D pseudo-color view and (f) 3D view of Zn microelectrode finger on PET substrate, showing the microelectrode thickness of 6.4 μm; photographs of flexible Zn//MnO_2 MBs with various shape diversity, including (g) individual interdigital structure, (h) 'DICP' logo-based Zn//MnO_2 MBs, and (i) an energy-storage pack of Zn//MnO_2 MBs connected in a tandem fashion of 5 series × 3 parallel; photographs of shape-designable Zn//MnO_2 MBs under different bending states, including (j) an individual interdigital Zn//MnO_2 MB, (k) tandem energy-storage packs via self-connection of (g) interdigital Zn//MnO_2 MBs in 5 series × 3 parallel bent at 180°, (l) four concentric-circle-shape, and (m) five linear-shape Zn//MnO_2 MBs in series, under flat and bending (180°) states.

= 8:1:1), only showed about 4 mAh/cm^3 after 100 cycles at 1 C (Fig. 3d), which definitely identify the superior performance of the Zn//MnO_2 planar MBs. Importantly, the defined discharge voltage platform of the GCD profiles was still well maintained (Fig. 3e), further demonstrating the outstanding structural stability of microelectrodes. In addition, the GCD profiles show that the capacity of planar MBs (15 mAh/cm^3) is much higher than stacked MBs (4 mAh/cm^3). Electrochemical impedance spectroscopy (EIS) revealed that the slope of Zn//MnO_2 planar MBs is much higher than the stacked cell at low frequencies (Fig. 3f, Fig. S8), indicative of the faster ion diffusion in the thinner microelectrodes of planar MBs. Furthermore, our Zn//MnO_2 MBs displayed exceptional long-term cycling stability, with a capacity retention of 83.9% even at a high rate of 5 C after 1300 cycles (Fig. 3g), outperforming most reported Zn//MnO_2 batteries, such as Zn//β-MnO_2 (75% retention after 200 cycles) [30], Zn//MnO_2@poly(3,4-ethylenedioxythiophene) (83.7% retention after 300 cycles) [33], yarn Zn//MnO_2 (98.5% retention after 500 cycles) [43], and Zn//MnO_2 (81.5% retention after 1000 cycles) [27]. The capacity decay was mainly attributed to the slow dissolution and disruption of the MnO_2 cathode, the volume changes of microelectrodes owing to the large size of Zn^{2+} insertion/extraction, and the concomitant stresses on account of the irreversible side reaction [44]. Also, the capacity fluctuation of Zn//MnO_2 MBs was mainly caused by the slow and non-uniform permeation of aqueous electrolyte into the electrodes during the cycling process. Several factors working together contributed to the outstanding electrochemical performance. First, metal-free graphene current collectors can significantly enhance the electrical conductivity of microelectrodes, and remarkably improve the rate capability of Zn//MnO_2 MBs. Secondly, compared with α-MnO_2 [45], the cathode of γ-MnO_2 with the mixed tunnels of

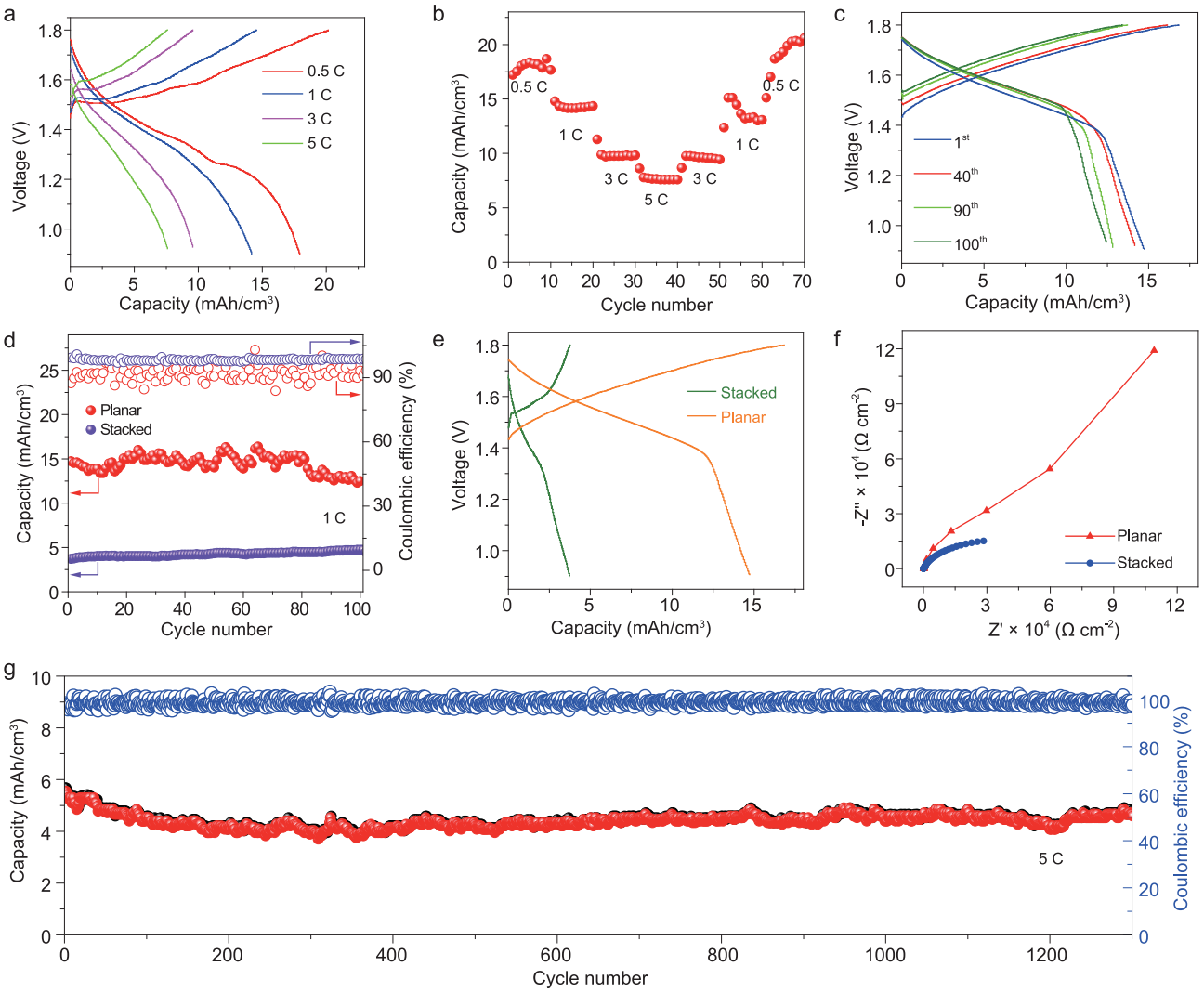

Figure 3. Electrochemical performance of printed Zn//MnO_2 planar MBs: (a) the GCD profiles, and (b) rate capability of Zn//MnO_2 MBs obtained from 0.5 C to 5 C; (c) the 1st, 40th, 90th, 100th GCD profiles, measured at a low rate of 1 C (15 mA/cm^3); (d) cycling stabilities of printed Zn//MnO_2 MBs with planar and sandwich-like stacked geometries, measured at a rate of 1 C; (e) the GCD profiles of the planar and stacked Zn//MnO_2 MBs; (f) EIS normalized to 1 of the planar and stacked Zn//MnO_2 MBs; (g) long-term cycling stability of Zn//MnO_2 planar MBs over 1300 cycles at a high rate of 5 C.

(1×1) and (1×2), is favorable for the Zn^{2+} ion intercalation/deintercalation in Zn//MnO_2 MBs, and also highly active to the proton, following the so-called two-step pathways in a mild electrolyte. Thirdly, the aqueous electrolyte containing Zn^{2+} with a Mn^{2+} additive has a high ionic conductivity of >1.0 S/cm, three orders of magnitude higher than organic electrolytes (10^{-3} S/cm) [46,47], thereby greatly hindering the pulverization and dissolution of MnO_2 and effectively improving the cyclability [48]. Last but not least, the polymer-assisted stable and conductive inks could substantially prevent the enormous volume change and the concomitant huge stress, thus contributing to the superior cyclability. As a result, the specific capacity and long-term cyclability of our Zn//MnO_2 MBs are much better than those reported Zn//MnO_2 batteries (Tables S1 and S2).

To properly understand the charge storage mechanism of Zn//MnO_2 MBs, we further examined the cyclic voltammetry (CV) curves tested at different scan rates (Fig. 4a). It is evident that the two pair redox peaks (1.6 vs. 1.35 V, and 1.52 vs. 1.22 V) of the CV curves became gradually broader with increasing scan rate, but their shapes stayed almost consistent (Fig. 4a). To obtain an insight into the intrinsic mechanism of Zn//MnO_2 MBs, we further analyzed the CV curves using the classic kinetics equations [49,50], $i = a\,v^b$ (or $\log i = \log a + b \log v$), where the current i obeys a power-rule relationship with the scan rate v. Both a and b are adjustable parameters. The value $b = 0.5$ indicates

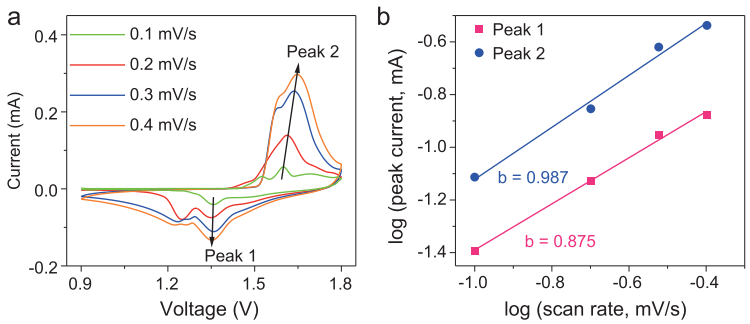

Figure 4. Kinetics analysis of ion intercalation of printed Zn//MnO_2 planar MBs: (a) CV curves of Zn//MnO_2 MBs obtained at various scan rates (v) from 0.1 to 0.4 mV/s; (b) plots of log (i) versus log (v) curves of cathodic and anodic peaks.

a diffusion-controlled insertion process, while a b value of 1.0 represents a surface capacitive process. In terms of this regulation, it is calculated that, for our Zn//MnO_2 MBs, the b values of four peaks are 0.875 (peak 1) and 0.987 (peak 2), respectively (Fig. 4b), indicating that the electrochemical kinetics of Zn//MnO_2 MBs mainly involved the surface capacitive process, accompanied by the diffusion-controlled intercalation process to some extent, contributing to the superior performance [1].

To meet the demands of future flexible and integrated microelectronics, developing flexible and integrated Zn//MnO_2 MBs is urgently required. To highlight this feature, we examined CV curves of Zn//MnO_2 MBs under varying bending angles from 0 to 180° at a scan rate of 1 mV/s (Fig. 5a). Apparently, it is confirmed that all the CV curves with typical battery behavior are well overlapped (Fig. 5b), along with an extraordinary capacity retention of almost 100% even when bent at 180° (Fig. 5c), suggestive of highly stable flexibility. This is attributed to the advance of the separator-free planar geometry of Zn//MnO_2 MBs built on one substrate, which can greatly enhance the intimate contact between the microelectrodes and flexible PET substrate, without involving the multiple interfacial delamination of stacked MBs [17].

Furthermore, the integrated Zn//MnO_2 MBs were constructed via connection of multiple cells in series and in parallel (Fig. 5d), free of metal-based interconnects. It is worth noting that, from the GCD profiles, Zn//MnO_2 MBs connected in series displayed analogical electrochemical properties, and simultaneously a stepwise increase of output voltage from 1.3 V for a single cell to 2.6 V for two cells and 3.9 V for three cells (Fig. 5e), suggestive of exceptional performance uniformity. Moreover, in a parallel fashion, the volumetric capacity of the integrated Zn//MnO_2 MBs connected from one to three cells increased progressively, while the output voltage stayed almost unchanged (Fig. 5f). Notably, a tandem pack of two serially connected Zn//MnO_2 MBs can readily power a light-emitting diode (LED) for a significantly long time under the flexible state, and light up a display screen of our institute 'DICP' logo, manifesting the enormous potential of our integrated Zn//MnO_2 MBs (Fig. 5g, h).

The volumetric energy density and power density are also important performance metrics to evaluate microscale energy-storage devices; therefore, a Ragone plot is shown to compare our Zn//MnO_2 planar MBs with other miniaturized energy-storage devices (Fig. 5i). Encouragingly, our printed Zn//MnO_2 MBs could output a maximum volumetric energy density of 17.3 mWh/cm^3 at a power density of 150 mW/cm^3. This energy density is much higher than the commercially available supercapacitors (SC: 1 mWh/cm^3), Zn-ion microsupercapacitors (Zn-MSC: 11.81 mWh/cm^3) [2], and lithium thin-film battery (10 mWh/cm^3) [51], ZnO//NiO (11 mWh/cm^3) [52], and NiO//Fe_3O_4 (1.83 mWh/cm^3) [53]. In addition, the power density of the Zn//MnO_2 MBs is 150 mW/cm^3, three orders of magnitude higher than a lithium thin-film battery (0.08 mW/cm^3). Therefore, our printed Zn//MnO_2 MBs not only manifest the merits of green, low-cost, scalable, and safe characteristics, but also possess high volumetric energy and power densities, making them suitable for numerous potential applications in miniaturized and printed electronics.

CONCLUSIONS

In summary, we have demonstrated the cost-effective and scalable fabrication of rechargeable printed Zn//MnO_2 planar MBs, with intriguing features of scalability, environmental benignity, high safety and metal-free current collectors, possessing high volumetric energy density, excellent rate capability and long-life cycling durability. Significantly, our printed Zn//MnO_2 MBs could be designed with various planar configurations, simultaneously representing designable artistic shapes, impressive flexibility, and remarkable modularization of building bipolar cells with high voltage and capacity output. More importantly, taking into the full considerations of low-cost and safe Zn, earth-abundant MnO_2, environmentally benign neutral aqueous electrolyte, and inexpensive screen-printing technology, our strategy of constructing printed Zn//MnO_2 MBs holds great potential as next-generation microscale power sources in various wearable, flexible, miniaturized and printed electronics [18].

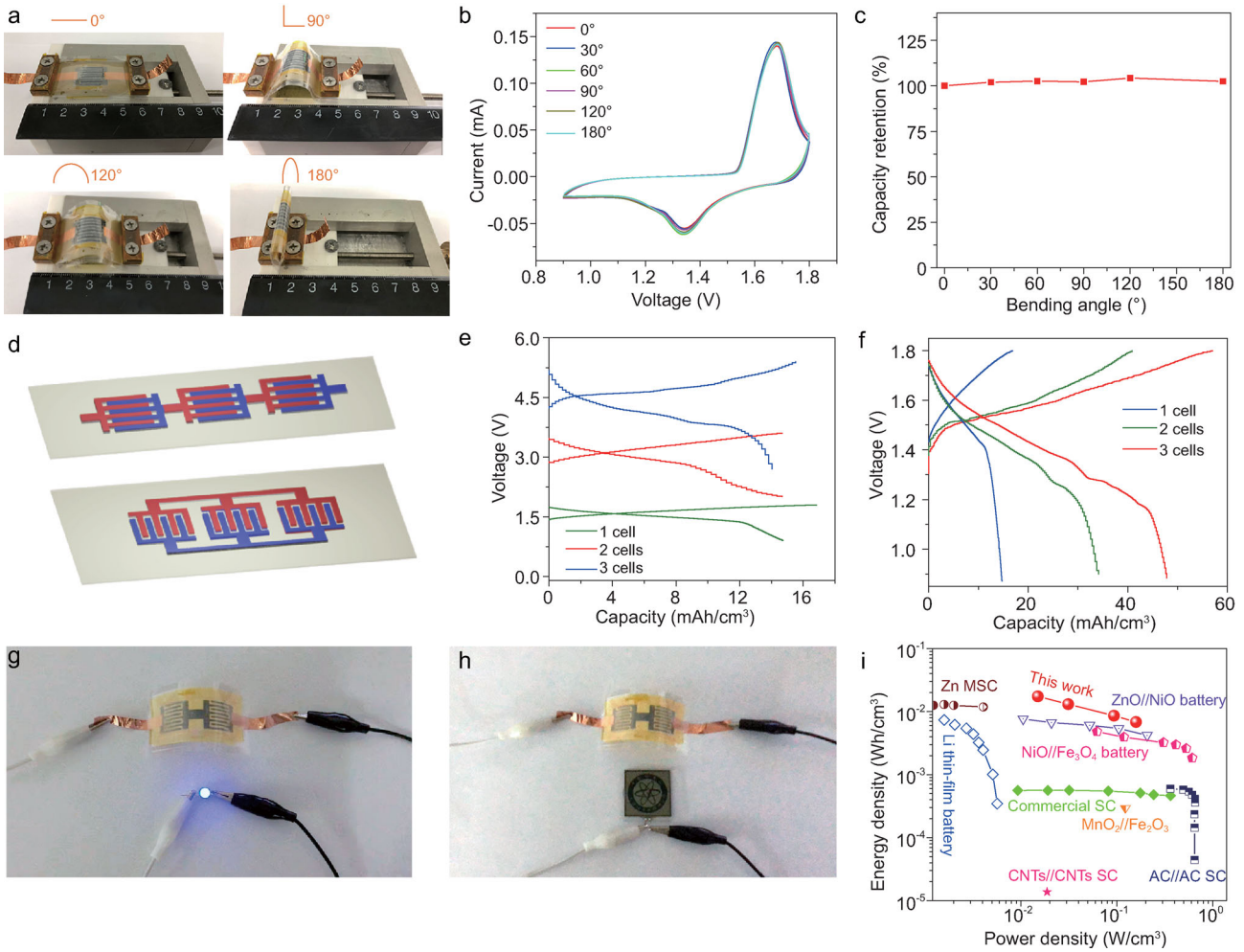

Figure 5. Exceptional flexibility and integration of Zn//MnO_2 planar MBs. (a) Photographs, (b) CV curves, and (c) capacity retention of Zn//MnO_2 MBs tested under different bending angles. (d) Schematic illustration of the integrated Zn//MnO_2 MBs connecting three cells in series (top) and in parallel (bottom). (e, f) GCD profiles of the integrated Zn//MnO_2 MBs connected in series (e) and in parallel (f) from 1 to 3 cells. (g, h) Photographs of two serially connected Zn//MnO_2 MBs, lighting up a LED (g), and powering a display of our institute 'DICP' logo (h) in a flexible state. (i) Ragone plot of Zn//MnO_2 MBs compared with other microscale energy-storage devices (AC: active carbon, CNTs: carbon nanotubes).

METHODS

Preparation of Zn ink and MnO_2 ink

Polyurethane resin (99%, Henan DaKen Chemical Co., Ltd) was added into the dispersant of aromatic solvents (S150, 98%, Pengchen New Material Technology Co., Ltd) and ethylene glycol diglycidyl ether (99%, Hangzhou Dayangchem Co., Ltd). To fully dissolve the resin, the mixture was heated to 80°C for 2 h. Subsequently, graphene (Nanjing XFNANO Materials Tech Co., Ltd), superfine graphite (Wuxi Hengtai Metal Material Co., Ltd), carbon black (90%, Zhengzhou Blue Ribbon Industry Co., Ltd) and MnO_2 powder (99.9%, Beijing DK Nano Technology Co. Ltd) were put into the above resin solution with an intense stirring of 1500 r/min for 30 min. After the resultant precursor was repeatedly ground under a three-roll grinder, MnO_2 ink was achieved. The mass proportion of polyurethane resin: graphene: superfine graphite: carbon black: MnO_2 powder is 3: 1: 1: 3: 2. The graphene conductive ink was prepared using the same reagent and procedure with graphene nanosheets (lateral size of 5–10 μm, 3–6 layers, Fig. S9), except with no addition of MnO_2. The Zn ink was made by uniformly mixing the as-prepared conductive ink and zinc powder (6–9 μm, 97.5%, Alfa Aesar) with a weight ratio of 2:1, when it was used.

Fabrication of Zn//MnO_2 MBs

Firstly, the highly conductive graphene ink was first printed on the PET, A4 paper, glass, or cloth substrates to form graphene-based current collectors and dried at 80°C in a vacuum box for 20 min

until totally dry. Secondly, Zn-based ink via the same approach was overlapped as anode on one side of the graphene-based current collectors, while MnO_2-based ink was subsequently deposited as cathode on the other side of the graphene-based current collectors. Then, the screen-printed asymmetric microelectrodes of Zn//MnO_2 MBs were dried at 80°C for 12 h. Afterwards, the neutral aqueous electrolyte of 2 M $ZnSO_4$ and 0.5 M $MnSO_4$ was slowly dropped onto the project area of the microelectrodes and packaged with Kapton tape. Finally, aqueous-based printed Zn//MnO_2 MBs were obtained. Note that the interdigital customized screen has eight fingers, with length of 12 mm, width of 1 mm and interspace of 1 mm (Fig. S10).

Materials characterization

The morphology, structure and composition of the active materials, graphene, the inks, and microelectrodes were analyzed using field-emission scanning electron microscopy (SEM, JSM-7800F), high-resolution transmission electron microscopy (HRTEM, JEM-2100), X-ray diffraction (XRD, X'pert Pro) (5–90°), four-point probe equipment (RTS-9), alpha step D-600, and thermogravimetric analysis (TGA, STA 449 F3) (measured at air atmosphere, 10°/min from 25 to 1000°C).

Electrochemical measurement

The CV curves obtained at varying scan rates of 0.1–0.4 mV/s and EIS tested from 100 kHz to 0.01 Hz with an AC amplitude of 5 mV were conducted by an electrochemical workstation (CHI 760E), and the GCD profiles were measured by a LAND CT2001A battery tester at voltages between 0.9 and 1.8 V at current densities from 0.5 to 5 C.

SUPPLEMENTARY DATA

Supplementary data are available at *NSR* online.

FUNDING

This work was supported by the National Natural Science Foundation of China (51572259, 51872283 and 21805273), National Key R&D Program of China (2016YFB0100100 and 2016YFA0200200), Liaoning Revitalization Talents Program (XLYC1807153), Natural Science Foundation of Liaoning Province (20180510038), Dalian Institute of Chemical Physics (DICP) (DICP ZZBS201708 and DICP ZZBS201802), Dalian National Laboratory For Clean Energy (DNL), Chinese Academy of Sciences (CAS), DICP & Qingdao Institute of BioEnergy and Bioprocess Technology (QIBEBT) (DICP&QIBEBT UN201702), DNL Cooperation Fund, CAS (DNL180310, DNL180308), Exploratory Research Program of Shaanxi Yanchang Petroleum (Group) Co., Ltd and DICP.

REFERENCES

1. Chao DL, Zhu C and Song M *et al.* A high-rate and stable quasi-solid-state zinc-ion battery with novel 2D layered zinc orthovanadate array. *Adv Mater* 2018; **30**: 1803181.
2. Sun GQ, Yang HS and Zhang GF *et al.* A capacity recoverable zinc-ion micro-supercapacitor. *Energy Environ Sci* 2018; **11**: 3367–74.
3. Kumar R, Shin J and Yin L *et al.* All-printed, stretchable Zn-Ag_2O rechargeable battery via hyperelastic binder for self-powering wearable electronics. *Adv Energy Mater* 2017; **7**: 1602096.
4. Choi K-H, Yoo J and Lee CK *et al.* All-inkjet-printed, solid-state flexible supercapacitors on paper. *Energy Environ Sci* 2016; **9**: 2812–21.
5. Hondred JA, Stromberg LR and Mosher CL *et al.* High-resolution graphene films for electrochemical sensing via inkjet maskless lithography. *ACS Nano* 2017; **11**: 9836–45.
6. Pan H, Shao Y and Yan P *et al.* Reversible aqueous zinc/manganese oxide energy storage from conversion reactions. *Nat Energy* 2016; **1**: 16039.
7. Wu ZS, Parvez K and Feng XL *et al.* Graphene-based in-plane micro-supercapacitors with high power and energy densities. *Nat Commun* 2013; **4**: 2487.
8. Wu ZS, Feng XL and Cheng HM. Recent advances in graphene-based planar micro-supercapacitors for on-chip energy storage. *Natl Sci Rev* 2014; **1**: 277–92.
9. Singh N, Galande C and Miranda A *et al.* Paintable battery. *Sci Rep* 2012; **2**: 5.
10. Deiner LJ and Reitz TL. Inkjet and aerosol jet printing of electrochemical devices for energy conversion and storage. *Adv Energy Mater* 2017; **19**: 1600878.
11. Sun K, Wei TS and Ahn BY *et al.* 3D printing of interdigitated Li-ion microbattery architectures. *Adv Mater* 2013; **25**: 4539–43.
12. McOwen DW, Xu SM and Gong YH *et al.* 3D-printing electrolytes for solid-state batteries. *Adv Mater* 2018; **30**: 1707132.
13. Ho CC, Murata K and Steingart DA *et al.* A super inkjet printed zinc—silver 3D microbattery. *J Micromech Microeng* 2009; **19**: 094013.
14. Hilder M, Winther-Jensen B and Clark NB. Paper-based, printed zinc—air battery. *J Power Sources* 2009; **194**: 1135–41.
15. Hu LB, Wu H and La Mantia F *et al.* Thin, flexible secondary Li-ion paper batteries. *ACS Nano* 2010; **4**: 5843–8.
16. Zheng S, Wu Z-S and Zhou F *et al.* All-solid-state planar integrated lithium ion micro-batteries with extraordinary flexibility and high-temperature performance. *Nano Energy* 2018; **51**: 613–20.
17. Zhao JW, Sonigara KK and Li JJ *et al.* A smart flexible zinc battery with cooling recovery ability. *Angew Chem Int Ed* 2017; **56**: 7871–5.
18. Wei TS, Ahn BY and Grotto J *et al.* 3D printing of customized Li-ion batteries with thick electrodes. *Adv Mater* 2018; **30**: 1703027.

19. Oudenhoven JFM, Baggetto L and Notten PHL. All-solid-state lithium-ion microbatteries: a review of various three-dimensional concepts. *Adv Energy Mater* 2011; **1**: 10–33.
20. Janoschka T, Hager MD and Schubert US. Powering up the future: radical polymers for battery applications. *Adv Mater* 2012; **24**: 6397–409.
21. Wang S, Wu ZS and Zheng S *et al.* Scalable fabrication of photochemically reduced graphene-based monolithic micro-supercapacitors with superior energy and power densities. *ACS Nano* 2017; **11**: 4283–91.
22. Xiao H, Wu Z-S and Zhou F *et al.* Stretchable tandem micro-supercapacitors with high voltage output and exceptional mechanical robustness. *Energy Storage Mater* 2018; **13**: 233–40.
23. Zheng S, Ma J and Wu Z-S *et al.* All-solid-state flexible planar lithium ion micro-capacitors. *Energy Environ Sci* 2018; **11**: 2001–9.
24. Zhou F, Huang H and Xiao C *et al.* Electrochemically scalable production of fluorine-modified graphene for flexible and high-energy ionogel-based microsupercapacitors. *J Am Chem Soc* 2018; **140**: 8198–205.
25. Wu ZS, Parvez K and Feng XL *et al.* Photolithographic fabrication of high-performance all-solid-state graphene-based planar micro-supercapacitors with different interdigital fingers. *J Mater Chem A* 2014; **2**: 8288–93.
26. Lai WH, Wang Y and Lei ZW *et al.* High performance, environmentally benign and integratable Zn//MnO_2 microbatteries. *J Mater Chem A* 2018; **6**: 3933–40.
27. Shi XY, Wu ZS and Qin JQ *et al.* Graphene-based linear tandem micro-supercapacitors with metal-free current collectors and high-voltage output. *Adv Mater* 2017; **29**: 1703034.
28. Xie BH, Wang Y and Lai WH *et al.* Laser-processed graphene based micro-supercapacitors for ultrathin, rollable, compact and designable energy storage components. *Nano Energy* 2016; **26**: 276–85.
29. Choi KH, Ahn DB and Lee SY. Current status and challenges in printed batteries: toward form factor-free, monolithic integrated power sources. *ACS Energy Lett* 2018; **3**: 220–36.
30. Islam S, Alfaruqi MH and Mathew V *et al.* Facile synthesis and the exploration of the zinc storage mechanism of β-MnO_2 nanorods with exposed (101) planes as a novel cathode material for high performance eco-friendly zinc-ion batteries. *J Mater Chem A* 2017; **5**: 23299–309.
31. Huang J, Wang Z and Hou M *et al.* Polyaniline-intercalated manganese dioxide nanolayers as a high-performance cathode material for an aqueous zinc-ion battery. *Nat Commun* 2018; **9**: 2906.
32. Wang Z, Ruan Z and Liu Z *et al.* A flexible rechargeable zinc-ion wire-shaped battery with shape memory function. *J Mater Chem A* 2018; **6**: 8549–57.
33. Zeng YX, Zhang XY and Meng Y *et al.* Achieving ultrahigh energy density and long durability in a flexible rechargeable quasi-solid-state Zn-MnO_2 battery. *Adv Mater* 2017; **29**: 1700274.
34. Zhang N, Cheng FY and Liu YC *et al.* Cation-deficient spinel $ZnMn_2O_4$ cathode in $Zn(CF_3SO_3)_{(2)}$ electrolyte for rechargeable aqueous Zn-ion battery. *J Am Chem Soc* 2016; **138**: 12894–901.
35. Xia C, Guo J and Lei Y *et al.* Rechargeable aqueous zinc-ion battery based on porous framework zinc pyrovanadate intercalation cathode. *Adv Mater* 2018; **30**: 1705580.
36. Song M, Tan H and Chao D *et al.* Recent advances in Zn-ion batteries. *Adv Funct Mater* 2018; **28**: 1802564.
37. Wang ZQ, Winslow R and Madan D *et al.* Development of MnO_2 cathode inks for flexographically printed rechargeable zinc-based battery. *J Power Sources* 2014; **268**: 246–54.
38. Gaikwad AM, Whiting GL and Steingart DA *et al.* Highly flexible, printed alkaline batteries based on mesh-embedded electrodes. *Adv Mater* 2011; **23**: 3251–5.
39. El-Kady MF and Kaner RB. Scalable fabrication of high-power graphene micro-supercapacitors for flexible and on-chip energy storage. *Nat Commun* 2013; **4**: 9.
40. Pech D, Brunet M and Durou H *et al.* Ultrahigh-power micrometre-sized supercapacitors based on onion-like carbon. *Nat Nanotechnol* 2010; **5**: 651–4.
41. Chmiola J, Largeot C and Taberna PL *et al.* Monolithic carbide-derived carbon films for micro-supercapacitors. *Science* 2010; **328**: 480–3.
42. Huang J, Guo Z and Ma Y *et al.* Recent progress of rechargeable batteries using mild aqueous electrolytes. *Small Methods* 2019; **3**: 1800272.
43. Li H, Liu Z and Liang G *et al.* Waterproof and tailorable elastic rechargeable yarn zinc ion batteries by a cross-linked polyacrylamide electrolyte. *ACS Nano* 2018; **12**: 3140–8.
44. Sun W, Wang F and Hou S *et al.* Zn/MnO_2 battery chemistry with H^+ and Zn^{2+} coinsertion. *J Am Chem Soc* 2017; **139**: 9775–8.
45. Wu B, Zhang G and Yan M *et al.* Graphene scroll-coated alpha-MnO_2 nanowires as high-performance cathode materials for aqueous Zn-ion battery. *Small* 2018; **14**: 1703850.
46. Ding J, Du Z and Gu L *et al.* Ultrafast Zn^{2+} intercalation and deintercalation in vanadium dioxide. *Adv Mater* 2018; **30**: 1800762.
47. Konarov A, Voronina N and Jo JH *et al.* Present and future perspective on electrode materials for rechargeable zinc-ion batteries. *ACS Energy Lett.* 2018; **3**: 2620–40.
48. Fu Y, Wei Q and Zhang G *et al.* High-performance reversible aqueous Zn-ion battery based on porous MnO_x nanorods coated by MOF derived N-doped carbon. *Adv Energy Mater* 2018; **8**: 1801445.
49. Chao D, Zhu C and Yang P *et al.* Array of nanosheets render ultrafast and high-capacity Na-ion storage by tunable pseudocapacitance. *Nat Commun* 2016; **7**: 12122.
50. Chao DL, Liang P and Chen Z *et al.* Pseudocapacitive Na-ion storage boosts high rate and areal capacity of self-branched 2D layered metal chalcogenide nanoarrays. *ACS Nano* 2016; **10**: 10211–9.
51. El-Kady MF, Strong V and Dubin S *et al.* Laser scribing of high-performance and flexible graphene-based electrochemical capacitors. *Science* 2012; **335**: 1326–30.
52. Liu J, Guan C and Zhou C *et al.* A flexible quasi-solid-state nickel–zinc battery with high energy and power densities based on 3D electrode design. *Adv Mater* 2016; **28**: 8732–9.
53. Zhao T, Zhang G and Zhou F *et al.* Toward tailorable Zn-ion textile batteries with high energy density and ultrafast capability: building high-performance textile electrode in 3D hierarchical branched design. *Small* 2018; **14**: 1802320.